PHOTODISSOCIATION AND RECOMBINATION OF THE OZONE MOLECULES

I.M. Sizova

P.N. Lebedev Institute of Physics,
Russian Academy of Sciences, Moscow
Received October 17, 1994

This overview summarizes the experimental and theoretical results obtained till 1992 on the UV dissociation and recombination of the ozone molecules. It provides information on the quantum yields of different dissociation channels and energy states of the fragments as well as on the role of the dissociation-recombination process in the anomalous enrichment of O_3 *with heavy isotopes observed in recent 10-15 years under both laboratory and atmospheric conditions.*

The O_3 molecule is an important subject for scientific studies due to its role in the atmosphere and its peculiar properties. In recent decades, much attention is being paid to studying the ozone, and interesting results have been obtained that open new directions for studies. That is why it is so urgent to compile the available information about the ozone properties. We have already overviewed, in Refs. 1-3, the results obtained till 1992 on O_3 electronic structure and absorption spectra from the near IR (ground state dissociation energy) to the far UV (O_3 ionization potentials). But we have not yet touched the problems on O_3 disintegration in the UV, the spectral range of a particular interest. During recent 10-15 years it emerges that the reserve reaction of O_3 recombination possesses a number of specific properties that are not still completely understood although they are characteristic not only of O_3 molecule. Below we present an overview of the literature published till 1992 concerning of the recombination-dissociation processes in gaseous ozone.

1. OZONE PHOTODISSOCIATION IN THE UV

The ozone disintegration energy is 1.05 eV (λ = 1181 nm), therefore, having absorbed the near IR radiation and shorter the O_3 molecule predissociates or dissociates into O + O_2 in different states depending on λ. In the range beyond the first two ionization potentials (IPs) (λ < 100 nm) it dissociates into more complex products, including ions of O, O_2, and O_3. Below 310 nm (~4 eV) O_3 has no allowed channels for disintegration into electronic-excited products, and they have not been observed in experiments. In the visible Chappuis band (620–540 nm), O_3 fragments with a unit quantum yield are produced in the ground states, although with nonequilibrium rotation-vibration distribution. This problem was reviewed in Ref. 2.

Starting from the Hartley band (λ < 310 nm), the main atmospheric absorption band, O_3 fragments are partially produced in excited electronic states. The UV absorption spectra of O_3 are described in detail in Ref. 3. Below we present the data on the quantum yields of different photodissociation channels and translation-rotation-vibration distribution of products.

1.1. Quantum yields of O_3 photodissociation products in the UV

The study of quantum yields of photodissociation channels and energy states of products is of interest from both practical and theoretical standpoints. In this respect the particular attention is paid to the Hartley band (310–220 nm) due to the importance of the process (O_3 here is the main natural source of excited atoms $O(^1D)$ and the availability of suitable sources of radiation (lasers) as well as because the O_3 molecule is relatively simple that permits the development of theoretical models, including *ab initio* ones.

Owing to the crossing of upper potential surface 1^1B_2 of the Hartley band and repulsive surface *R* (see Fig. 3 in Ref. 3), O_3 disintegrates in this band through two allowed channels: excited $O^* + O_2^*$ (with quantum yield φ^*) and unexcited $O + O_2$ ($\varphi = 1 - \varphi^*$) with the boundary at an interface between the Hartley and Huggins bands at $\lambda \simeq 308$–310 nm (for brevity hereinafter we use the following designations for the electronic states of O and O_2: $O \equiv O(^3P)$, $O^* \equiv O(^1D)$, $O^{**} \equiv O(^1S)$, $O_2 \equiv O_2(X^3\Sigma_g^-)$, $O_2^* \equiv O_2(a\,^1\Delta_g)$, $O_2^{**} \equiv O_2(b\,^1\Sigma_g^+)$; the quantum yields of the channels or individual products, $\varphi[\ldots]$, except for the aforementioned, are given in brackets). In the longer wave range, separate formation of O^* and O_2^* is energetically allowed (see Table I in Ref. 1). However, these channels are spin-forbidden, and they are not reliably observed in the experiments. No strict calculations for φ^* are still available in literature, because in order to do this one must solve the dynamic problem with regard to the interaction of all crossing surfaces. The experimental data on φ^*, from visible to far UV (the Chappuis, Huggins, Hartley bands and up to the first IPs), as well as few data on the quantum yields of other channels are presented in Fig. 1 and

0235-6880/95/09 682-18 $02.00

Table I (some data, in particular, for boundary $\lambda = 313$ nm, not included into the tables and plots, can be found in Refs. 9, 10, and 17). Shown in Fig. 1*a* and Table I*a* are the data of relative measurements of φ^*, whereas Fig. 1*b* and Table I*b* present the data of absolute measurements.

As seen, in the Hartley band at $\lambda < 300$ nm, φ^* smoothly depends on λ (it is practically constant about 0.8–0.9; in Ref. 38 the value 0.92 has been recommended), then sharply decreases at the band edge near 310 nm threshold, and at $\lambda > 320$ nm, in the Huggins bands, it is equal or very close to zero. How steep is the fall-off of φ^* and its position depend on the temperature[10] what is indicative of the role of rotation-vibration degrees of freedom in the dissociation dynamics. The data on possible smooth "tail" of $\varphi^*(\lambda)$ at $\lambda \geq 315$ nm, extending to 325 nm, are quite contradictory. It has been observed in the experiments reported in Refs. 15, 23, and 32 and has not been observed in the experiments reported in Refs. 10 and 13. The calculations,[32,38] generally speaking, confirm the presence of the tail, which is temperature-dependent and connected with the vibrations in O_3 content that are essential in the upper atmosphere ~100 km, where O_3 excitation exceeds the equilibrium level. In Ref. 34, devoted to CARS spectroscopy of O_2^* at O_3 UV photolysis, the fall-off of φ^* has not been observed up to 311 nm ($\varphi[O_2^*] = 0.89 \pm 0.03$ at $\lambda = 230$–311 nm). This disagreement with other data has been explained by the contribution from forbidden channels, the presence of which, however, has not been studied. Also obtained and justified in Ref. 34 is the isotopic dependence of φ^*.

For calculations of φ^* in the Hartley band [295–320 nm, 230–320 K (Ref. 10), 305–322 nm, 235 and 298 K and 313 nm, 200–320 K (Ref. 38)] simple threshold models with linear step were used that describe dissociation through the excited channel involving rotational-vibrational[10] (the step at the interval $\Delta E = 600$ cm^{-1}) and only rotational[10] ($\Delta E \simeq 800$ cm^{-1}) degrees of freedom. These models only roughly approximate the φ^* fall-off. The rest discrepancy with the experimental data (the temperature dependence of φ^* and $\varphi^* < 1$ at $\lambda < 300$ nm) is indicative of the role of interaction among the electronic, vibrational, and rotational motions. The threshold level itself also depends on the method used for φ^* calculation.[10] A many fold increase of φ^* has been observed in 259–315 nm region[24] under the excitation of the ozone $\nu_{1,3}$ modes with a CO_2 laser. However, in this case the measured parameter is the product of the cross section and φ^*, and therefore it is impossible to separate φ^* and its connection with the O_3 vibration.

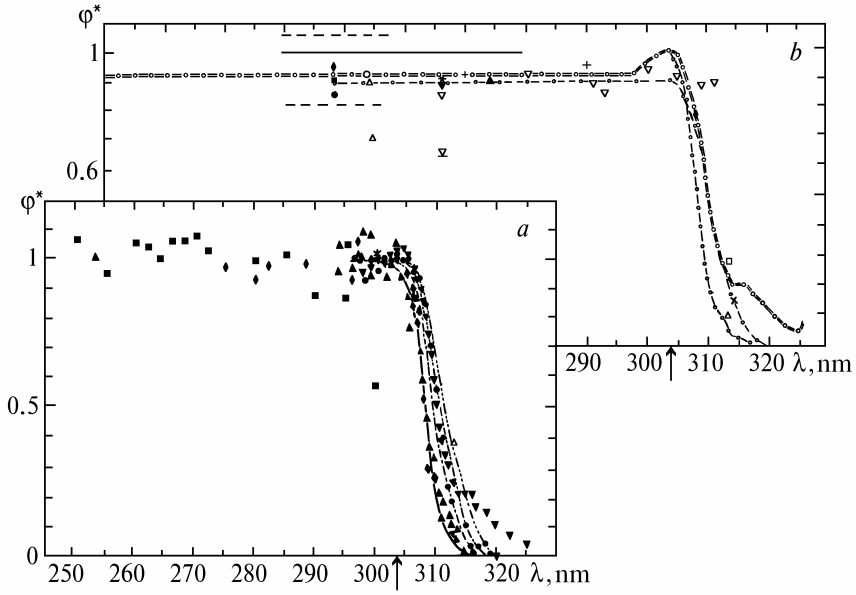

FIG. 1. Experimental and theoretical data on quantum yield $\varphi^*[O(^1D) + O_2(^1\Delta_g)]$ *in* O_3 *photodissociation in the Hartley band. Relative measurements (a):* 87.5 K, *1966, Ref. 4 (normalized to* 1 at $\lambda < 300$ nm*)* (Δ); 235 K, *1973/74, Ref. 5 (normalized to the average at* $\lambda = 270$–300 nm*)* (♦); 298 K, *1977, Ref. 13 (normalized to* 1 *at* $\lambda = 304$ nm*)* (•); 230 K (——); 263 K (–·–·); 298 K (–···–···); 320 K (–···– –), *1977, Ref. 12 (normalized to the average at* $\lambda < 300$ nm*)*; 296 K, *1978, Ref. 14 (normalized to the average at* $\lambda < 300$ nm*)* (■); *298 K, 1980, Ref. 15 (normalized to 1 at* $\lambda = 300$ nm*)* (▼). *Absolute measurements (b) (the energy threshold, according the calculations*[38] *equal to* 304 nm *is shown by arrow):* 296 K, *1970/71, Ref. 16* (Δ); 293 K, *1975, Ref. 17* ( ); 300 K, *1978, Ref. 19* (▲); *1979, Ref. 20* (×); *1980, Ref. 25* (*); *1980, Ref. 22* (–––); 298 K, *1982, Ref. 27* (■); *1982, Ref. 28* (+); 298 K, *1983, Ref. 29* (°); *1983, Ref. 31* (♦); 230 K (–·–·–) *and* 298 K (=·=·=) *1987, Ref. 32;* $^{32}O_2^*$ (∇) *and* $^{16}O^{18}O^*$ (C), *1987, Ref. 34;* 200–300 K, *1989, Ref. 36* (––·––).

TABLE Ia.

Experimental method			Radiation source; λ, nm	Δλ, nm	*T*, K	Quantum yields of other products φ[*M*]
Year, reference	Measurement technique, notes	Product being measured				
1966 Ref. 4	Control over pressure and O_3 by absorption; calculation by photochemical model, tables and plots vs. pressure are given		mercury lamp; 253.7 and 313.3	natural line-width	87.5 (liquid Ar)	
1970/71	Emission $O_2^* \rightarrow O_2$	O_2^*	253.7			$\varphi[O_2^{**}] \le 0.05$
Refs. 5-6	Emission $O_2^{**} \rightarrow O_2$	O_2^{**}				
1971	Emission $O_2^{**} \rightarrow O_2$	O_2^{**}	240–265			$\frac{\varphi[O_2^{**}]}{\varphi[O^*]} \le 0.05$
Ref. 7	Emission $O^* \rightarrow O_2$	O^*				
1973/74 Ref. 8	Measurement of quantum yield in reaction chain, given is only plot	O^*	mercury lamp 275–334	1.6	235	
1975/78 Refs. 9-11	Measurement of NO_2^* chemiluminiscence in reaction chain; given in Ref. 11 is the fitting formula $\varphi^*(\lambda, T)$	O^*	xenon lamp: 295–320	3.5	230; 263; 298; 320	
1977 Ref. 12	Measurement of NO_2^* chemiluminiscence in reaction chain	O^*	pulsed dye-laser Chromatix CMX-4 with frequency doubling: 293–316.5	0.15	298	
1977 Ref. 13	Measurement of NO_2^* chemiluminiscence in reaction chain	O^*	pulsed Rhodamine 6G dye-laser, frequency doubled in KDP; 295–320	0.1	298	
1978 Ref. 14	Measurement of NO_2^* chemiluminiscence in reaction chain; it is shown that $\varphi^* = \text{const} \pm 7\%$	O^*	pulsed dye-laser with doubling in Rhodamine *B*; 250–300	0.8	296	O_2^{**} was not observed
1980 Ref. 15	Measurement of NO_2^* chemiluminiscence in reaction chain	O^*	pulsed dye-laser Chromatix CMX-4 with doubling: 297.5–325	0.15	298	

TABLE Ib.

Experimental method			Radiation source	λ (Δλ), nm	*T*, K	Quantum yield φ* of channel $O^* + O_2^*$	Quantum yields of other products φ[*M*]
Year, reference	Measurement technique	Product being measured					
1970/71 Ref. 16	Control over pressure and O_3 by absorption; calculation by photochemical model; Emission $O_2^* \rightarrow O_2$	O_2^*	mercury lamp with filters	248; 254; 289/292; 297/303	296	0.9±0.2 in He and Ar; 0.7±0.2 in N_2	φ[O_2^*, O_2^{**}] = 1.0±0.1
		O^*		313	296	0.1±0.01	φ[O_2^{**}] ≤ 0.1
				334	296	≤ 0.02	
1975 Ref. 17	Control over pressure and O_3 by absorption; measurement of quantum yield of N_2 in reaction chain	O^*	a lamp with a chemical filter	313 (<1)	293 258 221	0.29±0.04 0.22±0.04 0.11±0.04	
1978 Ref. 18	Resonance absorption of O at λ = 130.2; 130.5 and 130.6 nm	O	KrF-laser	248		0.99±0.01	
1978 Ref. 19	Measurement of chemiionization of SmO; pass-time recording of kinetic energy	O^* and O	dye-laser Chromatix CMX-4 with and without frequency doubling	270–300	300	0.9 (274 nm) < 1 (276–300 nm)	
				600	300	0	
1979 Ref. 20	Mass-spectroscopic recording of $^{16}O^{18}O$	$^{18}O^*$	mercury lamp with filters of Cl_2 and $NiSO_4$–$CoSO_4$	230–280		1.00±0.05 for $^{54}O_3$	
1980 Ref. 21	Resonance absorption of O at λ = 130.2; 130.5 and 130.6 nm	O	KrF-laser	248		0.85±0.02	
1980 Ref. 22	Resonance absorption of 144.2; 148.6 and 126.3 nm; resonance fluorescence of O at ~ 130 nm; calculation by photochemical model	O_2^* and O	a lamp	240–257		1.06±0.31; 0.82±0.55	
1980 Ref. 23	Resonance absorption of O at ~ 130 nm;	O	4th harmonic of a Nd^{3+}: YAG laser	266		0.88±0.02	
1980 Ref. 24	Mass-spectroscopic recording of NO_2 in reaction chain	O^*	2nd harmonic of a dye-laser	314.5 (~ 0.18)	300	0.15±0.07	
1980 Ref. 25	Pass-time recording of kinetic energy	O_2	4th harmonic of a Nd^{3+}: YAG laser	266		~ 0.9	
1980 Ref. 26	Emission $XeO^* \rightarrow XeO$; control over O_3 by absorption; calculation by photochemical model	O^{**}	synchrotron radiation from Standford SPEAR	170–240 step 2.5			φ[O^{**}] < 0.001

TABLE Ib. (continued).

Experimental method			Radiation source	λ (Δλ), nm	*T*, K	Quantum yield φ* of channel $O^* + O_2^*$	Quantum yields of other products φ[*M*]
Year, reference	Measurement technique	Product being measured					
1982 Ref. 27			KrF-laser	248	298	0.907±0.028	
1982 Ref. 28				270		0.92±0.03	
				290		0.95±0.02	
1983 Ref. 29	Calculation by photochemical model		Mercury lamp with a monochromator	253.7 (10)	298	0.92±0.04;	
1983 Ref. 30	CARS spectroscopy of O_2	O_2	2nd harmonic of Nd^{3+}:YAG laser	532 (~0.006)	300	≤ 0.02–0.03	
	CARS spectroscopy of O_2^*	O_2^*		578±2 (~0.03)	300	≤ 0.02–0.03	
1983 Ref. 31	Resonance fluorescence of O at ~ 130 nm	O	KrF-laser	248		0.94±0.01	
			XeCl-laser	308		0.79±0.02	
1987 Ref. 32	Literature data			210–325.5	230	given is table	
					298	given is table	
1987 Ref. 33	Literature data			< 310		0.85±0.09	
1987 Ref. 34	CARS spectroscopy of $^{32}O_2^*$ and $^{16}O^{18}O^*$	O_2^*	2nd harmonic of dye laser and mixture of frequencies of Nd^{3+}:YAG and dye lasers	17 lines in the range 230–311 (0.001–0.002)	~ 300	table is given for 8 lines (see Fig. 1); on the average 0.89±0.03; at 266 nm $\varphi^*[^{34}O_2^*] \simeq \frac{3}{4}\varphi^*[^{32}O_2^*] \simeq 0.64$	$\varphi[O+O_2^*] \simeq 0$ O_2^{**} was not measured
1987 Ref. 35	CARS spectroscopy of O_2	O_2	dye laser pumped by Nd^{3+}:YAG laser	9 lines from the range 560–638	300	< 0.005	
CODATA 1989 Ref. 36	Literature data; the formula for $\varphi^*(\lambda = 300–320$ nm, $T)$ borrowed from Ref. 11 was used with a factor of 0.9			248–300	200–300	0.9±0.1	$\varphi[O^*+O_2^*] + \varphi[O+O_2] = 1.00$
				300–320	298	table is given	
1991 Ref. 37	Resonance fluorescence of O at λ = 130.2; 130.5 and 130.6 nm	O	ArF-laser	193	298±3	$\varphi^*[O^*] = 0.46±0.29$ or 0.75±0.44	$\varphi[O+O^*] = 1.20±0.15$ (i.e. three O atoms are produced in 12% of reactions) $\varphi[O] = 0.57±0.14$ $\varphi[O_2^{**}] = 0.50±0.38$
	Calculation by photochemical model	O^*					
			KrCl-laser	222	298±3	0.872±0.042	$\varphi[O] = 0.134±0.015$ $\varphi[O_2^{**}] \leq 0.03$

As a result, the data on φ^* available are odd, and not highly accurate, and they do not reflect the λ- and T-dependences completely. This does not permit more rigorous models to be constructed. Based on experimental data from Ref. 10, the empirical expression for $\varphi^*(\lambda, T)$ has been proposed in Ref. 11 for the Hartley and Huggins bands in 295–320 nm range at 230–320 K:

$$\varphi^*(\lambda, T) = A(\tau) \arctan(B(\tau) - (\lambda - \lambda_0(\tau))) + C(\tau) \ . \quad (1)$$

It agrees with the experimental data[10] within 1%. The expression (1) is truncated at the boundaries of the interval $0 \le \varphi^* \le 1$. Used in Eq. (1) are the following parameters: $\tau = T - 230$ K, $A(\tau) = 0.369 + 2.85\cdot10^{-4}\tau + 1.28\cdot10^{-5}\tau^2 + 2.57\cdot10^{-8}\tau^3$, $B(\tau)[\text{in nm}^{-1}] = -0.575 + 5.59\cdot10^{-3}\tau - 1.439\cdot10^{-5}\tau^2 - 3.27\cdot10^{-8}\tau^3$, $C(\tau) = 0.518 + 9.87\cdot10^{-4}\tau - 3.94\cdot10^{-5}\tau^2 + 3.91\cdot10^{-7}\tau^3$, $\lambda_0(\tau)$ [in nm] $= 308.20 + 4.4871\cdot10^{-2}\tau + 6.9380\cdot10^{-5}\tau^2 - 2.5452\cdot10^{-6}\tau^3$. This expression, being in good agreement with values recommended in Ref. 32 except only for the "tail", however needs validation.

Energetically, in the Hartly-Huggins bands, O^* and O_2^* may be produced via other channels (except $O^* + O_2^*$), spin-forbidden and so unlikely, as well as O^{**} and O_2^{**} (see Table I in Ref. 1). There are only few works directly devoted to estimation of the contributions from these channels, except the aforementioned indirect evidence from Ref. 34 and Ref. 33 that $\varphi[O^*]$ and $\varphi[O_2^*]$ disagree at $\lambda < 310$ nm, all of them are in favor of the $O^* + O_2^*$ channel. As was shown in Refs. 5–7, 16 based on the observation of emission due to the transitions $O_2^{**} \to O_2$ (762 nm), $O_2^* \to O_2$ (1270 nm), and $O^* \to O$ (630 nm), the probability of formation of O_2^{**} at $\lambda \le 253.7$ nm (Refs. 5, 6, and 16) and the ratio $\varphi[O_2^{**}]/\varphi[O^*]$ at $\lambda = 240$–265 nm (Ref. 7) are below 5% (the thresholds of the spin-forbidden channel, $O_2^{**} + O$, at 460 nm and the allowed one, $O_2^{**} + O^*$, at 260 nm). In Ref. 14, the absence of O_2^{**} was also shown at $250 \le \lambda \le 300$ nm. The validation given by the authors of Ref. 34 to the anomalously high yield $\varphi[O_2^*]$ observed in their experiment at $\lambda = 308$–311 nm (Fig. 1*b*) to be the result of a high yield $\varphi[O + O_2^{**}]$ at these wavelengths ($\simeq 0.56$ at $\lambda = 311$ nm) is unlikely to be considered other than controversial hypothesis.

It should be added that the data presented in Fig. 1 and Table I were obtained by recording not only O^*(Refs. 7, 8, 10–17, 19, 24, 31) and O_2^* (Refs. 5, 6, 16, 30, 34) but also O_2 (Refs. 25, 30, 35) and O (Refs. 18, 19, 21–23). Their agreement counts in favor of the proper choice of the dissociation mechanism. Although it has been proposed in Ref. 15 that the tail of φ^* at $\lambda > 312$ nm testifies that the spin-forbidden channel with a threshold at $\lambda \sim 410$ nm is possible, the authors have not tried to prove it. It was noted in Ref. 39 that the unequality $\varphi[O^*] < 1$ at $\lambda < 310$ nm is recognized to be more accurate than $\varphi[O_2^*] < 1$ at the same λ, and here the contribution from forbidden transitions of the type $O_3(X) \to O_3(2^3B_1)$ giving $\varphi[O_2^*] > \varphi[O^*]$ is possible, however quantitatively it was not proved.

Outside the Hartley band, at $\lambda < 200$ nm the allowed channel of O_3 dissociation with O^{**} production emerges (the thresholds for forbidden and allowed channels are 234 and 196 nm, respectively), however here O^{**} was not observed too. In particular, $\varphi[O^{**}]$ is below 0.1% for $\lambda = 170$–240 nm (Ref. 26) and below 3% of O^{**} yield in N_2O dissociation at atmospheric 121.6 nm L_α line (Ref. 40).

The measurements of yield of other neutral products in VUV are very odd, and they do not give an insight into the pattern. For example, in Ref. 41 it was obtained that at $\lambda = 157.6$ nm (F_2 laser) $\varphi[O] = 1.5$, $\varphi[O^*] = 0.55$ and $\varphi[O_2^{**}(v = 0$–$6)] = 0.5$ ($\varphi[v = 0] = \varphi[v = 1] = 0.10\pm0.03$; $\varphi[v = 2] = 0.09\pm0.03$; $\varphi[v = 3] = 0.08\pm0.025$; $\varphi[v = 4] = 0.06\pm0.02$; $\varphi[v = 5] = 0.04\pm0.015$; $\varphi[v = 6] = 0.03\pm0.015$; probably $\varphi[v > 6] \ne 0$, that agrees with the O_3 dissociation scheme:

$$O_3 + h\nu \xrightarrow{157.6\ \text{nm}} 3O, \quad \varphi = 0.45\ (\varphi[O] = 0.45\cdot3\,|\,1.5)$$
$$\longrightarrow O^* + O_2^{**},\ \varphi = 0.55. \quad (2)$$

Since it was obtained that $\varphi[O^*] = 0.55 > \varphi[O_2^{**}(v = 0$–$6)] = 0.5$, either a portion of O_2^{**} is produced at levels of v above six or the dissociation proceeds through other channels:

$$O_3 + h\nu \longrightarrow O^* + O_2^* \quad (\lambda_{\text{thres}} = 310\ \text{nm});$$
$$\longrightarrow O^* + O_2(c^1\Sigma_u^-)\ (\lambda_{\text{thres}} = 174\ \text{nm});$$
$$\longrightarrow O^* + O_2(B^3\Sigma_u^-)(\lambda_{\text{thres}} = 170\ \text{nm}),$$

although the emission of corresponding particles has not been observed. The formation of O_2 in O_3 photodissociation was first observed in Ref. 41.

The data obtained in Ref. 37, where the yields of O, O^*, and, respectively, O_2^{**} at the wavelengths of 193 nm (ArF laser) and 222 nm (KrCl laser) were measured, are qualitatively close to those from Ref. 41. The results obtained at 222 nm are close to the data obtained for the Hartley band at $\lambda < 310$ nm: $\varphi[O^*] = 0.872\pm0.042$, $\varphi[O] = 0.134\pm0.015$ (i.e., $\varphi[O^*, O] \simeq 1$ and $\varphi[O_2^{**}] \le 3\%$, whereas the results obtained at 193 nm wavelength are close to the data from Ref. 42 obtained for 157.6 nm: $\varphi[O^*] = 0.46\pm0.29$ (according to less accurate method, 0.75 ± 0.44), $\varphi[O] = 0.57\pm0.14$, $\varphi[O_2^{**}] = 0.50\pm0.38$, and total yield $\varphi[O^*, O] = 1.2\pm0.15$, i.e. greater than unity. All the above-said agrees, in general, with the scheme (2) with several different numbers: $\varphi[O^* + O_2^{**}] \simeq 50\%$, only in 12% of cases three atoms of O are produced, and the rest 40% cases are likely to correspond to the channel of unexcited products and $O^* + O_2^*$. As to the production of three atoms of oxygen, the authors of both Ref. 37 and Ref. 41 hold to the hypothesis about a two-step scheme rather than direct one: $O_3 + h\nu \to O + O_2 \to 3\,O$, where the second step is

due to the excess of internal energy of O_2. In other words, the data from Refs. 37 and 41 for $\lambda < 200$ nm can be considered as a result of the following process: at shorter λ in the UV the yield $O^* + O_2^*$ falls off, $O^* + O_2^{**}$ (threshold of 260 nm) appears, and the yield of $O + O_2$ grows, and in the latter case the portion of O_2 with a large internal energy, sufficient for uncollisional dissociation into atoms (O_3 two-step dissociation into 3O), increases. However, to construct the complete pattern in the UV, the experimental data for more than three wavelength are needed.

1.2. Energy states of photofragments

It is important to know energy states of the dissociation products both to understand the dissociation mechanism and estimate the quantum yields and the cross sections. Experimental data on the Hartley band are presented in Table II analogous to Table II from Ref. 2 for Chappuis band. As is seen, the photofragments are distributed nonuniformly over vibrations and rotations, and the major part of energy released in O_3 dissociation (>75%) converts to their translational energy.[34]

Valentini, in his first paper[44] concerning with the CARS spectroscopy of ozone photofragments, has shown that at $\lambda = 266$ nm in fragment molecules $^{32}O_2^*$ the even rotation quantum states are excited to a greater degree than the odd ones. As follows from the symmetry of states, all values of J are allowed for O_2^*, whereas for O_2 allowed are only the odd values of J. However, this does not explain the nonuniform distribution over J in $^{32}O_2^*$, since according to unpublished evidence by Pack (reference in Ref. 44) even if in the ozone photolysis separated will be O_2^* (90%) with only even J and O_2 (10%) with odd J, all J in O_2^* must mix when molecules flying apart. More recently, based also on collisional CARS spectra of O_2^* in O_3 photolysis, Valentini explained the suppression of J in findings of Refs. 34 and 44 by the symmetry limitations imposed on the dissociation process, crossing of surfaces, rather than on the dissociation products. The symmetry selection rules allow the transition from the channel $O_2^* + O^*$ to $O_2 + O$, i.e. the crossing of surfaces $^1B_2$ and R (see Fig. 3 in Ref. 3) only for states with odd J in symmetrical molecules $^{32}O_2^*$ and with any J in asymmetrical ones $^{16}O^{18}O^*$ that results in suppression of odd J in $^{32}O_2^*$ and its absence in $^{16}O^{18}O^*$. The authors of Ref. 34 studied the possibility of predominate production of Δ^+ component of Λ-doublet relative to Δ^- component, which may occur in O_3 photodissociation as it does in other molecules[34] and which also imposes a limitation on J (Δ^+ has only even values of J, whereas Δ^- has only odd ones, as well as the crossing of $^1B_2$ and R) to give the contribution into the suppression of odd J. However, the qualitative change of the distribution over J when going to isotopes for Λ-doublet differs from that due to surface crossing that allowed the authors of Ref. 34 to conclude that Λ-doublet does not influence the suppression of odd J. Thus, due to different symmetry of O_3 isotopes the surface crossing must be isotopically selective and the isotopic dependence of φ must be observed: for asymmetrical molecules $^{16}O^{17,18}O$ φ is twice as large as that for symmetrical molecules $^{32,36}O_2$ that was observed in Ref. 130 indeed.

The fact that surface crossing is of great importance in studying the dynamics of O_3 dissociation follows from Ref. 46. The authors of Ref. 46 made an attempt to calculate the distribution of rotational-vibrational energy in O_2^* using a single-channel model without regard for surface crossing. The result obtained for $\lambda = 266$ nm is even qualitatively inconsistent with the results from Ref. 25, it gives an extremum for $\nu = 1$, although the calculated absorption spectra well approximate the actual ones.

The nonuniform rotational-vibrational distribution of O_2^* in the Hartley band was obtained and qualitatively interpreted in Ref. 34. The vibrational distribution is practically λ-independent in 230–311 nm range and includes all energy-allowed values of J for a given λ with a sharp maximum at $\nu = 0$. It was interpreted by the authors with the use of the model of "adiabatic vibrational transition" and is due to the closeness of the bond lengths of oxygen atoms in O_3 ($R = 1.271$ Å) and O_2^* ($R = 1.215$ Å). The distribution over ν obtained in Ref. 34 agrees well with the distribution obtained in Ref. 25 with the use of different method for $\lambda = 266$ nm.

The O_2^* rotational distribution obtained in Ref. 34 possesses a pronounced nonuniform structure along with the suppression of odd J. Being practically as wide as the thermal distribution ($\Delta J^{\text{exp}}_{\text{HWHM}} \simeq 18$, $\Delta J^{300\ \text{K}}_{\text{therm}} \simeq 14$), it, in contrast to the thermal one, concentrates about the rather large values of J (for example, $J = 36$ for $\lambda = 240$ nm and $\nu = 0$) which decrease with ν and λ. The authors interpreted such a distribution satisfactorily using the simple "modified momentum rotational" model[47] accounting for initial rotation and bending vibration, ν_2, of the O_3 molecule. The idea of this model[45] is that photodissociation is considered as a result of instantaneous action of repulsive force, with a certain orientation, while the rotational distribution is governed by the laws of energy and momentum conservation. The role of potential surfaces reduces to the specification of direction of the aforementioned force (not necessarily along the bond break direction), and any interaction between fragments when flying apart is ignored.

The O_2^* rotational-vibrational distribution obtained in Ref. 34 proved to be close to O_2 distribution,[30,35,48] obtained by Valentini using CARS technique in the visible Chappuis band ($\lambda = 532$–638 nm) (see Ref. 2) and interpreted using the same models, as well as to the O_2 rotational distribution in the Hartley band, obtained recently in Ref. 45 with the use of the laser-induced fluorescence of O_2 ($\nu'' = 9$, 12, and 15). For a comparison,

TABLE II.

λ, nm, radiation source	Measurement technique, year, reference	$O_2(^3\Sigma_g^-) \equiv O_2$		$O_2(^1\Delta_g) \equiv O_2^*$		Atom translational energy, E	
		Vibrational states ν	Rotational states J	Vibrational states ν	Rotational states J	$O(^3P)$	$O(^1D)$
270–300 dye-laser Chromatix CMX-4	Measurement of SmO chemiionization and pass-time recording of kinetic energy 1978, Ref. 9	uniformly ν = 1–10		all allowed ν; given are distribution plots for λ = 271; 274; 290 and 302.5 nm	for λ = 302 nm the energy corresponds to classical flying-apart of two particles with equal momentum	2/3 of all energy with $f(\nu) \simeq \lvert A+\mathrm{coc}^2\nu \rvert$	2/3 of all energy with $f(\nu) \simeq \lvert A^*+\mathrm{coc}^2 N \rvert$
240–257	resonance fluorescence of O (~130 nm) and resonance absorption at 126.3; 144.2 and 148.6 nm; calculation by photochemical model 1980, Ref. 22			40±15% O_2^* with N = 0; 60±20% with N = 1–3			
266 4th harmonic of Nd^{3+}:YAG laser	pass-time recording of kinetic energy 1980 Ref. 25	wide range ν		all allowed ν; ν = 0/1/2/3 = = 57/24/12/7	for ν = 0 about 17% of total energy contains in rotation		
266 4th harmonic of Nd^{3+}:YAG laser Molectron MY34-20	resonance fluorescence of $O_3(1^1B_2)$; detection of O by the method of multiphoton ionization 1982 Ref. 44	resonance Raman scattering was observed; about 10^{-6} of molecules does not dissociate but fluoresce (l, 0, 2 m) into vibrational state of the ground electronic state of $O_3(X)$					
266 4th harmonic of Nd^{3+}:YAG and dye lasers	CARS spectroscopy of O_2^* 1983 Ref. 44			N = 0–3	$\frac{N(J_{\mathrm{even}})}{N(J_{\mathrm{odd}})} \simeq 0.6$ (N = 0) and 0.75 (ν = 1) ν = 2 and are not allowed		

TABLE II. (continued).

λ, nm, radiation source	Measurement technique, year, reference	$O_2(^3\Sigma_g^-) \equiv O_2$		$O_2(^1\Delta_g) \equiv O_2^*$		Atom translational energy, E	
		Vibrational states ν	Rotational states J	Vibrational states ν	Rotational states J	$O(^3P)$	$O(^1D)$
17 lines from 230–311 range 2nd harmonic of a dye laser and mixture of frequencies of a dye laser and Nd^{3+}:YAG laser	CARS spectroscopy of $^{16}O^{18}O^*$ and O_2^* 1987 Ref. 34	the spectrum was not observed due to distribution over great number of rovibrational states		all allowed ν: from ν = 0 at 311 nm to ν = 0–7 at 230 nm, with maxima at ν = 0; the distribution is practically λ-independent and corresponds to the adiabatic vibrational model	$\Delta J_{HWHM} \simeq \Delta J_{therm}^{300\ K} \simeq 18$; J_{max} are large (36 for ν = 0 and λ = 240 nm) and drop for higher ν; suppression of odd J_s in $^{32}O_2^*$, not in $^{34}O_2^*$; the distribution corresponds to the model of a singular rotational state		> 75% of the total energy generated
266.23±0.08 2nd harmonic of a dye laser Lambda Physik FL-2002	detection of O by pass-time technique and method of multiphoton ionozation 1990 Ref. 39	$\bar{\nu} = 12$; ν ≤ 23 were observed although energetically N up to 29 are allowed	on the basis of calculations,[47] it was taken $T_{rot} = 4 \cdot 10^3$ K			angular distribution with the anisotropy parameter β = 0.7±0.1; nonstatistical distribution of $O(^3P_j)$ over j = 0, 1, 2	
248 KrF laser Lamonics EX-510	laser-induced fluorescence of O_2(ν = 9,12, and 15) 1993 Ref. 45	observed were only ν = 9,12, and 15	narrow distributions with peaks: at ν = 9–14.5% of kinetic energy (J = 45), at ν = 12 ≃ 5.5%; at ν = 15 ≃ 4.7%				

the authors of Ref. 45 have calculated their rotational distribution using both the momentum model and the equilibrium statistical model and in the latter case the result appears to be qualitatively and quantitatively inconsistent with the experiment. It should be, however, noted that in Ref. 45 the momentum model allowing for O_3 rotation and vibration, well agreed with the rotational distribution, while being inconsistent with the angular distribution derived in Ref. 39. It is hard to say whether it is indicative of shortcomings of the model or improper choice of the configuration of the surface B^1A' (1^1B_2 with C_s symmetry), since choosing its parameters (and not the sole set) the results may be fitted to both the rotational and angular distributions at the same time.

1.3. Conclusions

The dissociation of O_3 in the Hartley band is due to crossing (interaction) of the four electronic surfaces: lower X^1A_1, two upper 1^1B_2 and 2^1A_1, and the repulsive R. In this case, the O_3 molecule being in X^1A_1 and R electronic states dissociates into $O + O_2$ whereas being in 1^1B_2 and 2^1A_1 states into $O^* + O_2^*$. Interaction of these surfaces gives rise to two channels of O_3 dissociation with the quantum yield of the excited channel, φ^*, having the shape of a step at the level 0.8–0.9 (the value recommended in Ref. 32 is 0.92) at $\lambda < 300$ nm with the fall-off down to zero near the threshold at 308–310 nm or, probably, with a tail extending up to 325 nm, depending on temperature and vibrational excitation of O_3. Practically no other channels of dissociation have been observed.[5–7,14,16,26] The analysis of φ^* and energy states of the products (having characteristic nonuniform rotational-vibrational distribution[19,25,34,44,45,49]) shows that the mechanism is too complicated and cannot be described adequately without regard for surface crossing,[10,34,38,46] their the symmetry, and isotopic dependence of φ^*. The O_2^* rotational-vibrational distribution in the Hartley band proved to be close to the O_2 distribution obtained using similar methods in the visible Chappuis band[30,35,48] and interpreted within the scope of the same models of "modified momentum rotation"[45,47] and "vibrational adiabatic transition".[45] More strict models for φ^* are not developed now, although the empirical analytical expression (1) has been proposed for $\varphi^*(\lambda, T)$ and experimental data have been qualitatively interpreted with a satisfactory adequacy.

In the shorter wave portion of the UV ($\lambda < 200$ nm) the data on quantum yields were obtained only at three wavelengths, 222, 193, and 157.6 nm, that does not allow the justified conclusions to be drawn. The energy states of the dissociation products at $\lambda < 200$ nm have not yet been investigated.

2. RECOMBINATION OF THE OZONE MOLECULES

2.1. Rate of recombination

The reaction of three-particle recombination of ozone molecules,

$$O + O_2 + (M) \xrightarrow{k_r^M} \begin{matrix} \xrightarrow{a} O_3 + (M) + 106.5\ \text{kJ/mole}, \\ \xrightarrow{b} O_3^* + (M) \end{matrix} \qquad (3)$$

is the main source of O_3 in the atmosphere and laboratories. We use the designation O_3^* for the lower excited electronic state or one of them ($1^3B_{1,2}$, 1^3A_2, 2^1A_1). Small contribution from ion-molecular reactions[32] and reactions of electronic-excited molecules to the formation of O_3 may partly be important only in the upper atmosphere (≥100 km). Therefore considerable attention has been recently focused on the reaction (3). Recent data on k_r under low pressure (<10 atm), where it is the third-order reaction, $k_{r,0}$, are presented in Table III (for earlier data see reviews). Under high pressure, when k_r is the second-order reaction, $k_{r,\infty}$, it depends on buffer gas and, probably on temperature. For example, at $T = 200$–300 K and $p \simeq 200$ atm $k_{r,\infty}^{N_2} = (2.8 \pm 1.5)10^{-12}$ cm^3/s (Ref. 50), and in Ref. 51 it was obtained that $k_{r,\infty}^{O_3} : k_{r,\infty}^{NO_3} : k_{r,\infty}^{NO_2} \simeq 1:2:6$.

In the intermediate pressure region under not very high temperature, the constant can be presented in the form of Lindemann-Hinshelwood expression multiplied by a factor F (Ref. 36):

$$k_r = k_{r,0} \frac{1}{1 + [M]/[M_c]} F\ , \qquad (4)$$

where $[M]$ is the current concentration of M, and $[M_c] = k_{r,\infty}/([k_{r,0}/[M])$ is the concentration at the point of crossing of the extrapolation curves for $k_{r,0}$ and $k_{r,\infty}$ as functions of $[M]$. The broadening parameter F depends on pressure,

$$\log F \simeq \log F_c/[1 + \log^2([M]/[M_c])],$$

and, via F_c, on temperature. The parameter F_c, as a function of temperature, can be approximately presented, according to the Troe procedure,[36] in the form

$$F_c = a \exp(-T/T^*) + \exp(-T^{**}/T) + \\ + (1 - a) \exp(-T/T^{***}), \qquad (5)$$

where it is generally believed that $a = 1$ and $T^{**} = 4T^*$. In this case, at room temperature, the second term in the right-hand side of Eq. (5) gives only a small contribution. Just this approximation for F_c was proposed in the review CODATA of 1982, Ref. 50. Then for the aforementioned reaction $k_{r,\infty}^{N_2}$ in 200–300 K temperature range $[M_c](298\ \text{K}) \simeq 5 \cdot 10^{21}$ cm^{-3}, $a = 1$, $T^* = (1800 \pm 800)$ K, and $F_c(298\ \text{K}) = 0.85 \pm 0.10$. In the

review CODATA of 1989, Ref. 36, new expression for F_c at 200-300 K was proposed, which also is the approximation of Eq. (5): $F_c = \exp(-T/696)$, i.e. $T^* = 696$ K, $a = 1$, the second term in Eq. (5) was neglected, and $F_c(298\ \text{K}) = 0.65\pm0.10$.

In Ref. 52, $k_r^{\text{Ar, He, N}_2}$ as functions of p and T were studied at temperature 85–373 K and pressure 1–1000 atm. At low T, $k_r(p)$ bents with increasing p in accordance with Eq. (4). At high T, the curve $k_r(p)$ is S-shaped. Four k_r mechanisms at high pressures were discussed, namely, the energy transfer, the radical complex, the recombination into the excited electronic state of O_3, and the diffusion mechanism. The competition among these mechanisms well explains the observed $k_r(p, T)$ dependences. Discussed also was the constant of reaction in the transient region from gas to liquid.

At low pressure (see Table III), the molecules of O_3, produced in $k_{r,a}$, are vibrational-excited. According to Ref. 53, no less than 80% of O_3 molecules are excited: about 20% of reaction exothermity goes into the excitation of ν_1 and ν_3 vibrational modes ($\overline{\nu}_1 \simeq \overline{\nu}_3 \simeq 0.8$, $\overline{\nu}_{1,3} \simeq 1.6$) and about 30% goes into the ν_2 mode ($\overline{\nu}_2 \simeq 3.7\pm0.8$). According to Ref. 54, the ν_1 mode is not excited, and, following Ref. 55, excited is mainly the ν_3 mode (up to $\nu = 5$) and the ν_1 mode is excited weakly (up to $\nu = 1$), whereas the ν_2 mode is not excited at all. According to Ref. 53, in $k_{r,b}$ O_3^* is also excited: $\overline{\nu}_{1,3} \simeq 0.011$.

By the room temperature we usually mean the temperature range 293–308 K and, most often, the temperature of 298 K. Just this value is used in the column T in Table III as the room temperature, unless otherwise indicated. The temperature dependence is given in Table III either in the Arrenius form, $k = A\exp(-\Delta/T)$, with a dash in the column headed n, or in the form $k = A(-\Delta/T)^n$, and then all columns are filled. In some cases, several different constants borrowed from reviews 32 and 36 are presented.

TABLE III.

M	A, cm^6/s	Δ, K	n	T, K	k_r under room temperature, cm^6/s	Year, reference
			$k_{r,a}$			
O_2[1)]	$5.0\cdot10^{-37}$	2940	–	298 293–1000 298	$0.44\ k_{r,a}(O_3)$ $2.6\cdot10^{-41}$ $(0.42\pm0.08)k_r$	1983 Ref. 29 1983 Ref. 56 1987 Ref. 57
			$k_{r,b}$			
				298	$0.62\ k_{r,b}(O_3)$ $(0.58\pm0.08)k_r$	1980 Ref. 58 1987 Ref. 57
			k_r			
O_3	$4.6\cdot10^{-35}$	−1050	–		$1.56\cdot10^{-33}$	1979/80 Refs. 59, 60
O_3	$1.43\cdot10^{-33}$ $4.65\cdot10^{-34}$	300 300	2.0 1	200–300 200–300	$2.27\ k_r(O_2)$ $1.45\cdot10^{-33}$ $4.66\cdot10^{-34}$	1987 Ref. 32
O_2	$(6.75\pm0.43)\cdot10^{-35}$	−635±18	–	262–340	$5.69\cdot10^{-34}$	1979/80 Refs. 59, 60
O_2	$2.15\cdot10^{-34}$ $(6.9\pm1.0)\cdot10^{-34}$	−345±60 300	– 1.25±0.2	219–368	$(6.8\pm1.0)\cdot10^{-34}$[2)]	1980 Ref. 61
O_2	$(6.40\pm0.60)\cdot10^{-35}$ $(5.96\pm0.34)\cdot10^{-34}$	−663±26 300	– 2.37±0.32	218–353	$(5.71\pm1.63)\ 10^{-34}$	1982 Ref. 62
O_2				298	$6.07\cdot10^{-34}$	1983 Ref. 29
O_2	$5.96\cdot10^{-34}$	300	2.37		$6.06\cdot10^{-34}$	1988 Ref. 63
O_2	$6.2\cdot10^{-34}$	300	2.0±0.5	200–300	$6.2\cdot10^{(-34\pm0.1)}$	1989 Ref. 36
O	$2.15\cdot10^{-34}$ $2.52\cdot10^{-34}$	−345 −1057	– –	200–300 200–300	$6.84\cdot10^{-34}$ $8.75\cdot10^{-33}$	1987 Ref. 32
N_2	$(1.82\pm0.23)\cdot10^{-35}$	−995±37	–	263–298	$5.13\cdot10^{-34}$	1979/80 Ref. 59, 60
N_2	$8.82\cdot10^{-35}$ $(6.2\pm0.9)\cdot10^{-34}$	−575±60 300	– 2.0±0.5	219–368	$(6.1\pm1.0)\cdot10^{-34}$[2)]	1980 Ref. 61

TABLE III. (continued)

M	A, cm^6/s	Δ, K	n	T, K	k_r under room temperature, cm^6/s	Year, reference
			k_r			
N_2	$(5.04\pm1.52)\cdot10^{-35}$ $(5.70\pm0.19)\cdot10^{-34}$	-724 ± 94 300	– 2.62 ± 0.18	218–366	$(5.75\pm0.24)\cdot10^{-34}$	1982 Ref. 62
N_2					$0.39\ k_r(O_3)$	1983 Ref. 29
N_2				298	$0.9\ k_r(O_2)$	1987 Ref. 57
N_2	$5.70\cdot10^{-34}$	300	2.62		$5.80\cdot10^{-34}$	1988 Ref. 63
N_2	$5.7\cdot10^{-34}$	300	2.8 ± 0.5	200–300	$5.7\cdot10^{(-34\pm0.1)}$	1989 Ref. 36
N_2	$5.5\cdot10^{-34}$ $5.2\cdot10^{-34}$	300 1000	2.6 1.3	100–400 700–900	$5.6\cdot10^{-34}$	1990 Ref. 52
Ar	$(6.24\pm1.53)\cdot10^{-35}$	-525 ± 70	–	262–340	$3.63\cdot10^{-34}$	1979/80 Refs. 59, 60
Ar	$6.6\cdot0^{-35}$	-510 ± 23	–	200–346	$3.65\cdot10^{-34}$	1980 Ref. 58
Ar	$6.30\cdot0^{-35}$ $(3.9\pm0.5)\cdot0^{-34}$	-535 ± 70 300	– 1.9 ± 0.3	219–368	$(3.8\pm1.0)\cdot10^{-34}$ [2]	1980 Ref. 61
Ar					$2.6\cdot10^{-34}$	1981 Ref. 65
Ar	$(3.68\pm0.82)\cdot0^{-35}$ $(3.81\pm0.28)\cdot0^{-34}$	-687 ± 70 300	– 2.54 ± 0.40	220–353	$(3.97\pm0.36)\cdot10^{-34}$	1982 Ref. 62
Ar	$\sim 2\cdot10^{-32}$			80		1987 Ref. 55
Ar				298	$0.6\ k_r(O_2)$	1987 Ref. 57
Ar	$8.0\cdot10^{-33}$ $4.5\cdot10^{-34}$ $4.0\cdot10^{-35}$	100 300 1000	3.2 2.7 1.0	80–150 150–400 700–1000	$4.0\cdot10^{-34}$	1990 Ref. 52
CO_2	$3\cdot10^{-32}$	-520	–		$1.72\cdot10^{-31}$	1979 Ref. 66
CO_2					$(1.37–1.5)\cdot10^{-33}$ [3]	1979 Ref. 20
He				300	$2.83\cdot10^{-34}$	1981 Ref. 67
He				298	$(3.47\pm0.12)\cdot10^{-34}$	1982 Ref. 62
He					$0.34\ k_r\ (O_3)$	1983 Ref. 29
He	$3.48\cdot10^{-34}$	300	1.9	219–368	$3.5\cdot10^{-34}$	1984 Ref. 68
He					$\approx 0.6\ k_r\ (O_2, N_2)$	1987 Ref. 32
He	$7.2\cdot10^{-33}$ $3.4\cdot10^{-}34$	100 300	3.7 1.2	100–200 200–1000	$3.4\cdot10^{-34}$	1990 Ref. 52
SF_6					$(2.12–2.17)\ k_r\ (O_3) =$ $= (2.25–3.4)\cdot10^{-33}$	1983 Ref. 29
Kr				298	$4.9\cdot10^{-34}$	1972 Ref. 64
CO				298	$(4.42–6.7)\cdot10^{-34}$	1972 Ref. 64
N_2O				298	$(0.88–1.5)\cdot10^{-33}$	1972 Ref. 64
H_2O				298	$(6.0\pm5.5)\cdot10^{-33}$	1972 Ref. 64
CF_4				298	$(1.6\pm0.1)\cdot10^{-33}$	
Air=21%	$1.07\cdot10^{-34}$ $(6.3\pm0.9)\cdot10^{-34}$	-525 ± 60 300	– 1.9 ± 0.5	219–368	$6.2\cdot10^{-34}$ [2]	1980 Ref. 61
O_2+79%	$5.15\cdot10^{-35}$ $(3.81\pm0.28)\cdot10^{-34}$	-635 ± 52 300	– 2.54 ± 0.40	220–353	$5.67\cdot10^{-34}$	1982 Ref. 62
N_2	$6.0\cdot10^{-34}$	300	2.3	200–300	$6.1\cdot10^{-34}$	1987 Ref. 97

[1] Theoretical investigation of the reaction $O + O_2 + O_2 \rightarrow O_3 + O_2^*$.

[2] Arrenius representation of temperature dependence is more accurate.

[3] Constants are given for the reactions of isotopes $^{16,18}O + {}^{18}O^{18}O + M$ and $^{16}O + {}^{16}O^{18}O + M$.

2.2. Isotopic enrichment of the ozone

During the last decade, a new feature of the ozone media has been revealed, namely, the enrichment of O_3 with heavy isotopes as compared to natural composition, including the mass corrections to it. Anomalous content of O_3 isotopes received the name of non-mass-dependent (NMD) effect in contrast to usual mass-dependent (MD) one, which is accounted for by differences in velocities and vibrational distribution functions (frequencies) of molecules with different masses. The ratio of enrichment of asymmetrical and symmetrical $^{50}O_3$ isotopes also proved to be nonstatistical. These effects are observed under both atmospheric and laboratory conditions and are characteristic of not only O_3 but also of some other symmetrical molecules, namely, CO_2 and S_2F_{10}.

The isotopic enrichment of the atmospheric ozone was first predicted in Ref. 69 in 1980. But, this prediction has collapsed and has came under criticism in the following Refs. 70–72. However, in the same year the anomalous O_3 isotopic composition was experimentally observed in the stratosphere,[73] what stimulated the remote and contact measurements in the stratosphere[74–79] as well as in laboratories and the theoretical studies.[80–93]

Usually, the enrichment is described in terms of δ-terms expressing (in % or ‰) the deviation of a sample isotopic composition from the standard:

$$\delta^{17,\,18}O = \left(\frac{^{17,\,18}R_{obs}}{^{17,\,18}R_{stand}} - 1\right)\cdot(100\%\ \text{or}\ 1000‰)\ ,$$

where $^{17,\,18}R = {}^{17,\,18}O/{}^{16}O$ or similar relation for the basic and rare isotopes of O_3. The standard natural content of oxygen isotopes is 0.204% ^{18}O and 0.0037% ^{17}O of all oxygen atoms that gives for the most abundant isotopic specie of ozone, $^{50}O_3$, 0.408% for the asymmetrical molecule, $^{50}O_{3,\,asym} \equiv {}^{16}O^{16}O^{18}O$, and 0.204% for the symmetrical molecule, $^{50}O_{3,sym} \equiv {}^{16}O^{18}O^{16}O$, of all O_3 (Refs. 42, 78). In accordance with MD effect, the following relation

$$\delta^{17}O = 0.52\ \delta^{18}O \qquad (6)$$

must take place, and, in addition, statistically the content of $^{50}O_{3,\,asym}$ and $\delta^{50}O_{3,\,asym}$ must be twice as much as those for symmetrical modifications.

The measurement results on altitude profiles of $\delta^{17,18}O$ for atmospheric ozone are shown in Fig. 2, whereas altitude average data for the stratosphere and laboratory results are listed in Table IV. The stratospheric enrichment proved to be rather large, up to 45% at an altitude about 40 km, and, moreover the relation (6) and the statistical ratio of asymmetrical isotopic species to symmetrical ones[76,78] were not valid. The degree of enrichment observed under laboratory conditions for different ways of producing O_3 from O_2, O_3, and their mixtures turned out to be markedly lower than most of the stratospheric findings (5–14%). The cause of this discrepancy is not yet understood. The atmospheric enrichment, being calculated from laboratory data, proves to be underestimated,[92] and the lack of experiments on atmospheric enrichment, with parallel, *in situ* and in laboratory, handling of samples does not allow solution to the problem on the adequacy of different measurement techniques.

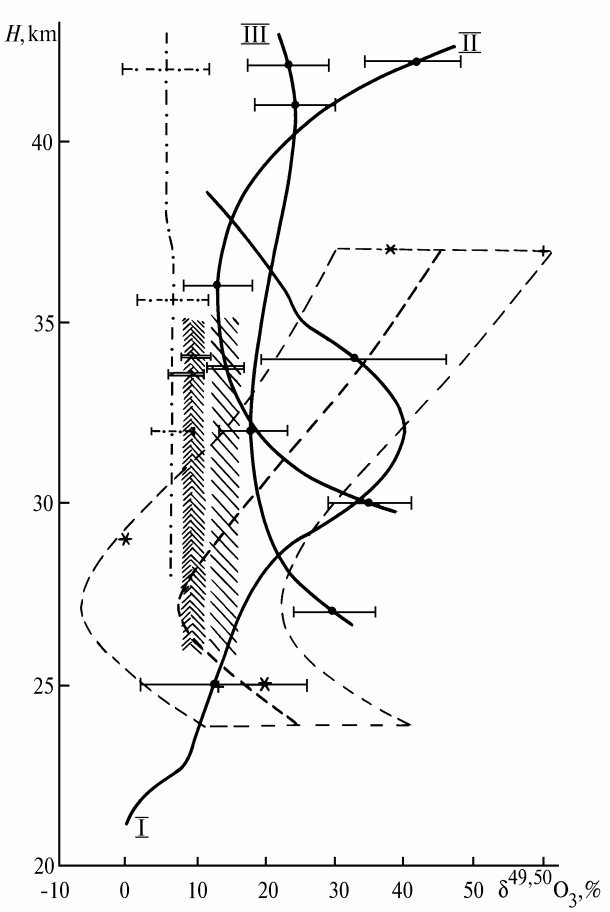

FIG. 2. Altitude distribution of the degree of atmospheric ozone enrichment with heavy isotopes. A part of the figure was borrowed from Ref. 76. Solid lines is for the data of night (September 4, 1980, Ref. 73(I) and day (June 7, 1982, Ref. 74(II) and July 18, 1983, Ref. 74(III)) mass-spectroscopy measurements of $\delta^{50}O_3 \simeq \delta^{49}O_3$ *from balloons; bold dashed line is for data of* $\delta^{50}O_3$ *measurements from thermal IR solar radiation from balloon, borrowed from Ref. 76:* $\delta^{50}O_{3,\,sym}(+)$ *and* $\delta^{50}O_{3,\,asym}(-)$*; dot-and-dash line is for the data of* $\delta^{50}O_{3,\,sym} \simeq \delta^{50}O_{3,\,asym}$ *measurements by IR-radiation, from Ref. 77; shaded parts are for the data of laboratory mass-spectroscopy processing of six balloon cryogenic samples, from Ref. 79:* $\delta^{50}O_3$, 1 *flight* (\\), $\delta^{50}O_3$, 1 *flight* (\\), $\delta^{50}O_3 \simeq \delta^{49}O_3$, 2–3 *flights* (//).

In laboratory experiments, the NMD effect and nonstatistical ratio of the asymmetrical species of $\delta^{50}O_3$ to the symmetrical ones is about four rather than two.[94] In practice, instead of the ratio (6), it was observed that $\delta^{17}O \simeq \delta^{18}O$. Generally speaking, the value $m = \delta^{17}O/\delta^{18}O$ depends on pressure, temperature, initial conditions of ozone dissociation, etc., as the value $\delta^{18}O$. The experiments on studying the T- and p-dependences of $\delta^{18}O$ and m are listed in Table V together with their results. Reference 92 reports on study of the enrichment of all O_3 isotopes from $^{49}O_3$ ($^{17}O^{32}O_2$) to $^{54}O_3$ as a function of p, T, and molecular symmetry. It was shown there that the enrichment strongly depends on the molecular symmetry ($\delta^{16}O^{17}O^{18}O \simeq 21\%$ whereas $\delta^{17}O^{17}O^{17}O$ and $\delta^{18}O^{18}O^{18}O$ proved to be somewhat below the statistical values).

As was already noted, the original, photodissociation, theory of the O_3 enrichment[69] was not confirmed.[70–72] Most laboratory experiments showed that enrichment occurs not at the O_3 or O_2 dissociation, but at the stage of recombination. In these experiments, O_3/O_2 mixtures were analyzed with known composition of isotopes which dissociate due to different causes under conditions controlled in time and in kinetic energy with the succeeding recombination of O_3 (Refs. 88–92). In such a way, with the help of kinetic models, the roles of different elementary processes in isotopic effect were revealed. The results are presented in Table VI. From the findings of Ref. 90, the reaction $O + O_3 \rightarrow 2O_2$ does not depend on the isotopic composition of reagents and is not related to the enrichment of O_3. At the same time, the collisional dissociation $O_3 + M \rightarrow O_2 + O + M$ and recombination, both yield enrichment (~5% and up to 10%, respectively, to the same degree for ^{17}O and ^{18}O). This conclusion is intriguing for two reasons. First, it contradicts the general statistical theory of monomolecular dissociation (Troe, 1977) both in the magnitude of the effect (much greater) and in sign (enrichment rather than depletion). And, second, since inverse reactions yield the close isotopic effects of the same sign, they are not thermodynamically and statistically inverse, i.e. they are nonequilibrium. The theories available just emphasize the leading role of this nonequilibrium along with the quantum-mechanic effects and symmetry.

TABLE IV.

Experiment	In the atmosphere			In laboratory					
	Ref. 75 from the ground	Ref. 78 from the ground and balloons		Ref. 84	Ref. 85	Ref. 86	Ref. 87	Ref. 88	Ref. 90
H, km	entire ozone layer	> 37	< 37						
$\delta\ ^{50}O_{3,sym}$, %	5±7	16–20							
$\delta\ ^{50}O_{3,asym}$, %	11±11	25–40							
$\delta\ ^{50}O_3$, %		20–33	0±20	~8–10	~8.5	~9–14	~9–12	~8	~5

TABLE V.

Experiment	Ref. 81		Ref. 84	Ref. 86	Ref. 87	Ref. 92
T, K	≃ 200				127–360	
p	1–152 Torr (pure O_2)	19–423 Torr (O_2 + He)	1–30 Torr	0.8–0.87 atm (pure O_2)	5–1000 Torr	
Analyzed parameters	$\delta^{18}O$; m	m	m	$\delta^{18}O$; m	$\delta^{18}O$	$\delta^{49-54}O_3$
Results	at $p \geq 2$ Torr $m = 1.01\pm0.02$ at $p = 1$ Torr $m = 0.720$	$m = 0.99\pm0.01$	$m = 1$ at $p > 20$ Torr and decreases at $p < 20$ Torr due to heterogeneous processes at walls	$\delta^{18}O \simeq 8.98\%$ at 0.8 atm, exponentially decreases at 1–20 atm down to ≃ 1.04% at 35 atm and goes to a constant at $p \geq 56$ atm; decrease in k_r does not correlate with $\delta^{18}O$ with increasing $^r p$; $m = 1$ within the accuracy of 99%	$\delta^{50}O_3 \simeq 10–12\%$ at $T = 298$ K ≃ 9–10% at $T = 250$ K	

TABLE VI.

	Experimental conditions of a laboratory experiment			Role of the primary process in Refs. 88–91		
	Thermal dissociation of O_3 20–30°C Ref. 91 90–110°C Ref. 90	Visible photolysis of O_3 532 nm Refs. 88, 90	UV photolysis of O_3 180–260 nm Ref. 91 254 nm Ref. 90	Photodissociation of O_3	Recombination of O_3	Collisional dissociation of O_3
$\delta^{17}O$, %				–(1.5–2.2)	5–10	≃ 5
$\delta^{18}O$, %				–(2.8–3.6)	5–10	≃ 5
m	≃ 1	≃ 0.53	≃ 0.65			

TABLE VII.

Authors, reference, year	Explanation for NMD effect	
	Model	Results
Kaye (Ref. 71, 1986)	dynamic statistical model Troe + reactions of isotopic exchange during the process of O_3 recombination	very small enrichment, opposite sign
Heidenreich, Thiemens (Ref. 81, 1986)	symmetry properties of O_3 + difference in stability of transient activated complexes of O_3 isotopomers in the process of recombination	right sign of enrichment; according to Bates, Refs. 93, 95, the symmetry gives MD effect
Bates (Refs. 93, 95, 1988–1990)	symmetry properties of O_3 + finiteness of the rate of energy randomization of transient energy complex + flip process during O_3 recombination	explanation of NMD effect, if $\nu_d \simeq \nu_f$; $\nu_d \simeq 1.6\ \nu_r$; $\nu_d \simeq 2.8_{10}12\ s^{-1}$ and depends slightly on pressure (by the factor of 1.5 at p = 1–100 atm)
Valentini (Ref. 42, 1987)	symmetry of crossing of O_3 potential electronic surfaces in the Hartley band, selection rules in nonadiabatic reactions	Good quantitative explanation for all peculiarities observed experimentally[71,80,81]; explanation for enrichment both in reaction of recombination and in thermal dissociation; the necessity of further development of the model for stratospheric conditions

The most of enrichment theories and of the enrichment anomalies start from the reaction k_r. The most appropriate among them is the Bates model,[93,95] which allows for the symmetry and the finiteness of the rate of randomization of transient activated complex energy with O_3 generation as well as the so-called flip-processes, or rearrangement of isotopic atoms, when an outer atom breaks from the central one and adds to the other outer atom. According to Bates, the recombination and isotope exchange should be considered in a unified nonequilibrium reaction chain. If there are several channels of complex generation and dissociation, then the NMD effect takes place once the frequencies of randomization ν_r, dissociation ν_d ($\nu_r/\nu_d \geq 0.3$), and rearrangement ν_f are comparable. The available experiments are explicable by the model from Ref. 93 with the frequencies being in the ratio: $\nu_f = \nu_d$, $\nu_d = 1.6\nu_r$, and $\nu_d \approx 2.8 \cdot 10^{12}\ s^{-1}$ at a low pressure ~1 atm with a weak pressure-dependence (increases by a factor of 1.21 at 10 atm and by a factor of 1.48 at 100 atm).

Much less attention was paid to revealing of the role of O_3 dissociation in enrichment, which also may be large, see Table VII. Only the work by Valentini[42] may be noted here, which explains in some detail the contribution from O_3 recombination and dissociation into the enrichment. The idea is that in the dissociation the ground electronic state $X^3\Sigma_g^-$ of O_2 is enriched with isotopes to the degree, as the first metastable electronic state $^1\Delta_g$ is depleted, that results in the enrichment of O_3 during recombination since only $O_2(X)$ takes part in it.

The Valentini model is based on the data on rotational-vibrational distribution of oxygen in O_3 products in the Chappuis and Hartley bands, obtained by the uncollisional CARS spectroscopy of O_2, O_2^*, and their isotopic species[30,34,35,44,48] (see above and Refs. 1–3). In the Hartley band, where O_3 dissociates into $O + O_2$ and $O^* + O_2^*$ with isotope-dependent quantum yield, in view of the symmetry of $^{32}O_2$ and the asymmetry of the main isotopes $^{17,18}O^{16}O$, the equal NMD enrichment of O_2 and depletion of O_2^* with both isotopes occur due to symmetry influence on the crossing of the band's potential surfaces: the upper one 1^1B_2 with the outcome of $O^* + O_2^*$ and repulsive one R with the outcome of $O + O_2$. In Ref. 42 the conclusion was drawn about the possible existence of a number of nonadiabatic processes connected with the symmetry and surface crossing, leading to NMD separation of isotopes, an example of which is the O_3 photodissociation, as well as, in view of the interaction of these surfaces, the quenching reaction $O_2^* + M \rightarrow O_2 + M$. Using this model, Valentini has calculated the enrichment of O_3 in O_2 discharge in experiments reported in Refs. 80, 81 and has obtained a good quantitative agreement with the experiment and p- and T-dependences consistent with the experimental ones. The model allows for the main reactions, including isotopic exchange. Under low pressure (<3 Torr) the calculational results agree with the opposite-sign effect from Ref. 71. However, in the stratospheric conditions the Valentini model is not so successful, since in the oxygen-nitrogen medium the isotope separation between O_2^* and O_2 dissipates much earlier than they can be bounded by a chemical process. The mechanisms of a more complex chain involving C-H cycles are likely to take part here, that probably leads to the difference in the atmospheric and laboratory enrichment.

The process of oxygen isotopic exchange are included in the Valentini and Bates models. But they are, as a rule, poorly studied. In this connection, a start has been made in Ref. 96 with their study and refinement of their role in enrichment.

It is most likely that the pattern presented is incomplete. The authors of Ref. 92, for example, believe that lower electronic states of O_3, especially $^3B_2$, may play an important role in the enrichment.

2.3. Conclusions

The reaction k_r of O_3 recombination, in addition to the production of nonequilibrium excited molecules, possesses also the isotopic selectivity, i.e., its rate depends on isotopic composition and symmetry of a molecule produced. This dependence is such that the composition of molecules produced not only differs from the isotopic composition of O, but can be accounted for neither by different mass of isotopes nor by the statistical symmetry properties.

The NMD enrichment of O_3 with heavy isotopes has been first observed in 1980 is the stratospheric mass-spectroscopy measurements from baloons,[73] and then it has been observed many times both in the atmosphere[74–79] and in laboratory.[80–92] In the atmosphere $\delta^{17}O^{18}O$ has reached 45% at an altitude ≃ 40 km, whereas in laboratory it has proved to be much lower, about 14%, and the reason for this discrepancy is not clearly understood. In laboratory experiments, it has been shown that both enrichment and the ratio $\delta^{17}O/\delta^{18}O$ depend, generally speaking, on the experimental conditions and the way of O_3 and O_2 dissociation from the initial mixture.[81,84,86–88,90–92]

The attempts to separate the contributions from different processes in enrichment have shown that "enriching" reactions are the reaction k_r and, probably, its inverse, the O_3 collisional dissociation.[88–91] The most appropriate model of k_r (Refs. 93 , 95) is based on the symmetry, the presence of flip-process, and the finiteness of the rate of energy randomization of the transient activated complex, comparable with the rates of its disintegration and flip reaction. Of interest is the hypothesis by Valentini[42] that enrichment is the result of influence of isotope symmetry on the crossing of O_3 potential surfaces and selection rules in the nonadiabatic processes. Valentini succeeded in quantitative explanation of a number of laboratory data,[71,80,91] but to be applied under atmospheric conditions his model needs the inclusion of some additional reaction chains.

In addition to ozone, the isotopic enrichment was also observed in several symmetric molecules, namely, CO_2 and S_2F_{10}.

REFERENCES

1. I.M. Sizova, Atmos. Oceanic Opt. **6**, No. 5, 301–312 (1993).
2. I.M. Sizova, Atmos. Oceanic Opt. **6**, No. 8, 533–546 (1993).
3. I.M. Sizova, Atmos. Oceanic Opt. **7**, No. 5, 303–316 (1994).
4. W.B. DeMore and O.F. Raper, J. Chem. Phys. **44**, No. 5, 1780 (1966).
5. M. Gauthier and D.R. Snelling, Chem. Phys. Lett. **5**, 93 (1970).
6. M. Gauthier and D.R. Snelling, J. Chem. Phys. **54**, 4317 (1971).
7. R. Gilpin, H.I. Schiff, and K.H. Welge, J. Chem. Phys. **55**, 1087 (1971).
8. C.-L. Lin and W.B. DeMore, J. of Photoch. **2**, 161 (1973, 1974).
9. G.K. Moortgat and P. Warneck, Z. Naturforsch **30a**, 835 (1975).
10. G.K. Moortgat, E. Kudszus, and P. Warneck, J. Chem. Soc. Far. Trans. 2. **73**, 1216 (1977).
11. G.K. Moortgat and E. Kudszus, Geoph. Res. Lett. **5**, No. 3, 191 (1978).

12. D.L. Philen, R.T. Watson, and D.D. Davis, J. Chem. Phys. **67**, No. 7, 3316 (1977).
13. I. Arnold, F.J. Comes, and G.K. Moortgat, Chem. Phys. **24**, 211 (1977).
14. P.W. Fairchild and E.K.C. Lee, Chem. Phys. Lett. **60**, No. 1, 36 (1978).
15. J.C. Brock and R.T. Watson, Chem. Phys. **46**, 477 (1980).
16. I.T.N. Jones and R.P. Wayne, Proc. Roy. Soc. Lond. **A319**, 273 (1970), **A321**, 409 (1971).
17. S. Kuis, R. Simonaitis, and J. Heicklen, J. Geophys. Res. **80**, 28 (1975).
18. S.T. Amimoto, A.P. Force, and J.R. Wiesenfeld, Chem. Phys. Lett. **60**, No. 1, 40 (1978).
19. C.E. Fairchild, E.J. Stone, and G.M. Lawrence, J. Chem. Phys. **69**, No. 8, 3632 (1978).
20. O. Kajimoto and R.J. Cvetanovich, Int. J. Chem. Kinet. **11**, 605 (1979).
21. S.T. Amimoto, A.P. Force, J.R. Wiesenfeld, and R.H. Young, J. Chem. Phys. **73**, No. 3, 1244 (1980).
22. O. Klais, A.H. Laufer, and M.J. Kurylo, J. Chem. Phys. **73**, No. 6, 2696 (1980).
23. J.C. Brock and R.T. Watson, Chem. Phys. Lett. **71**, No. 3, 371 (1980).
24. P.F. Zittel and D.D. Little, J. Chem. Phys. **72**, No. 11, 3900 (1980).
25. R.K. Sparks, L.R. Carlson, K. Shobatake, et al., J. Chem. Phys. **72**, No. 2, 1401 (1980).
26. L.C. Lee, G. Black, R.L. Sharpless, and T.G. Slange, J. Chem. Phys. **73**, No. 1, 256 (1980).
27. P.H. Wine and A.R. Ravishankara, Chem. Phys. **69**, No. 3, 365 (1982).
28. J.E. Davenport, FAA Technical Report EE-80-44-REV, Federal Aviation Administration, Office of Environment and Energy, Washington, DC, AD A117 502, 1982.
29. C. Cobos, E. Castellano, and H.J. Schumacher, J. Photoch. **21**, 291 (1983).
30. D.S. Moore, D.S. Bomse, and J.J. Valentini, J. Chem. Phys. **79**, No. 4, 1745 (1983).
31. G.D. Greenblatt and J.R. Wiesenfeld, J. Chem. Phys. **78**, No. 12, 4924 (1983).
32. J.I. Steinfeld, S.M. Adler-Golden, and J.W. Gallagher, J. Phys. Chem. Ref. Data **16**, No. 4, 911 (1987).
33. R.P. Wayne, Atm. Envir. **21**, No. 4, 1683 (1987).
34. J.J. Valentini, D.P. Gerrity, D.L. Phillips, et al., J. Chem. Phys. **86**, No. 12, 6745 (1987).
35. H.B. Levene, J.-C. Nieh, and J.J. Valentini, J. Chem. Phys. **87**, No. 5, 2583 (1987).
36. R. Atkinson, D.L. Baulch, R.A. Cox, et al., J. Phys. Chem. Ref. Data **18**, No. 2, 881 (1989).
37. A.A. Turnipseed, G.L. Vaghjiani, T. Gierczak, et al., J. Chem. Phys. **95**, No. 5, 3244 (1991).
38. S.M. Adler-Golden, E.L. Schweitzer, and J.I. Steinfeld, J. Chem. Phys. **76**, No. 5, 2201 (1982).
39. T. Kinugawa, T. Sato, T. Arikawa, et al., J. Chem. Phys. **93**, No. 5, 3289 (1990).
40. B.A. Ridley, R. Atkinson, and K.H. Welge, J. Chem. Phys. **58**, 3878 (1973).
41. M.R. Taherian and T.G. Slanger, J. Chem. Phys. **83**, No. 12, 6246 (1985).
42. J.J. Valentini, J. Chem. Phys. **86**, No. 12, 6757 (1987).
43. D.G. Imre, J.L. Kinsey, R.W. Field, and D.H. Katayama, J. Phys. Chem. **86**, No. 14, 2564 (1982).
44. J.J. Valentini, Chem. Phys. Lett. **96**, No. 4, 395 (1983).
45. W.J. Daniels and J.R. Wiesenfeld, J. Chem. Phys. **98**, No. 1, 321 (1993).
46. M.G. Sheppard and R.B. Walker, J. Chem. Phys. **78**, No. 12, 7198 (1983).
47. H.B. Levene and J.J. Valentini, J. Chem. Phys. **87**, No. 5, 2594 (1987).
48. J.J. Valentini, D.S. Moore, and D.S. Bomse, Chem. Phys. Lett. **83**, No. 2, 217 (1981).
49. W.M. Jones and N. Davidson, J. Am. Chem. Soc. **84**, No. 15, 2868 (1962).
50. D.L. Baulch, R.A. Cox, P.J. Crutzen, et al., J. Phys. Chem. Ref. Data **11**, No. 2, 327 (1982).
51. V.H. Hippler and J. Troe, Zeitsch. Electroch. Ber. Bunsen. Phys. Chem. **75**, No. 1, 27 (1971).
52. V.H. Hippler, R. Rahn, and J. Troe, J. Chem. Phys. **93**, No. 9, 6560 (1990).
53. C.W. Von Rosenberg and D.W. Trainor, J. Chem. Phys. **61**, No. 6, 2442 (1974); **63**, No. 12, 5348 (1975).
54. T. Kleindienst, J.B. Burkholder, and E.J. Bair, Chem. Phys. Lett. **70**, No. 1, 117 (1980).
55. W.T. Rawlins, R.A. Armstrong, and G.E. Caledonia, J. Chem. Phys. **87**, No. 9, 5202; 5209 (1987).
56. M.P. Popovich, Yu.V. Filippov, and S.N. Tkachenko, Vestn. Mosk. Univ., Khimiya **24**, No. 6, 546 (1983).
57. J.R. Locker, J.A. Joens, and E.J. Bair, J. Photoch. **36**, No. 3, 235 (1987).
58. T. Kleindienst, J.R. Locker, and E.J. Bair, J. Photoch. **12**, No. 1, 67 (1980).
59. I. Arnold and F.J. Comes, Chem. Phys. **42**, 231 (1979).
60. I. Arnold and F.J. Comes, J. Mol. Struct. **61**, 243 (1980).
61. O. Klais, P.C. Anderson, and M.J. Kurylo, Int. J. Chem. Kinet. **12**, No. 7, 469 (1980).
62. C.L. Lin and M.T. Leu, Int. J. Chem. Kinet. **14**, No. 4, 417 (1982).
63. W.F. Evans, I.C. McDade, J. Yuen, and E.J. Llewellyn, Can. J. Phys. **66**, 941 (1988).
64. R.E. Huie, J.T. Herron, and D.D. Davis, J. Phys. Chem. **76**, No. 19, 2653 (1972).
65. J.W. Keto, C.F. Hart, and C.-Y. Kuo, J. Chem. Phys. **74**, No. 8, 4433 (1981).
66. V.A. Krasnopolsky and V.A. Parshev, Planet. Space Sci. **27**, 113 (1979).
67. J.P. Burrows, R.A. Cox, and R.G. Derwent, J. Photoch. **16**, 147 (1981).

68. H.E. Elsayed-Ali and G.H. Miley, IEEE J. Quant. El. **QE20**, No. 8, 977 (1984).
69. R.J. Cicerone and J.L. McCrumb, Geoph. Res. Lett. **7**, 252 (1980).
70. J.A. Kaye and D.F. Strobel, J. Geophys. Res. **88**, 8447 (1983).
71. J.A. Kaye, J. Geoph. Res. **91**, No. D7, 7865 (1986).
72. A.J. Blake, S.M. Gibson, and D.C. McCoy, J. Geoph. Res. **89**, 7277 (1984).
73. K. Mauersberger, Geophys. Res. Lett. **8**, 935 (1981).
74. K. Mauersberger, Geophys. Res. Lett. **14**, No. 1, 80 (1987).
75. C.P. Rinsland, V.M. Davi, J.-M. Flaud, et al., J. Geoph. Res., No. 90, 10719 (1985).
76. M.M. Abbas, J. Guo, B. Carli, et al., J. Geoph. Res. **92**, No. D11, 13231 (1987).
77. B. Carli and J.H. Park, J. Geoph. Res. **93**, No. D4, 3851 (1988).
78. A. Goldman, F.J. Murcray, D.G. Murcray, et al., J. Geoph. Res. **94**, No. D6, 8467 (1989).
79. B. Schuler, J. Morton, and K. Mauersberger, Geoph. Res. Lett. **17**, No. 9, 1295 (1990).
80. J.E. Heidenreich III and M.H. Thiemens, J. Chem. Phys. **78**, 892 (1983).
81. J.E. Heidenreich III and M.H. Thiemens, J. Chem. Phys. **84**, No. 4, 2129 (1986).
82. S.K. Bains-Sahota and M.H. Thiemens, J. Phys. Chem. **91**, 4370 (1987).
83. R.K. Sander, T.R. Loree, S.D. Rockwood, and S.M. Freund, Appl. Phys. Lett. **30**, 150 (1977).
84. M.H. Thiemens and T. Jackson, Geoph. Res. Lett. **14**, No. 6, 624 (1987).
85. M.H. Thiemens and T. Jackson, Geoph. Res. Lett. **15**, 639 (1988).
86. M.H. Thiemens and T. Jackson, Geoph. Res. Lett. **17**, No. 6, 717 (1990).
87. J. Morton, J. Barnes, and B. Schuler, J. Geoph. Res. **95**, No. D1, 901 (1990).
88. J. Wen and M.H. Thiemens, EOS Transact. **7**0, No. 43, 1034 (1989).
89. J. Wen and M.H. Thiemens, Chem Phys. Lett. **172**, No. 5, 416 (1990).
90. J. Wen and M.H. Thiemens, J. Geoph. Res. **96**, No. D6, 10911 (1991).
91. S.K. Bhattacharya and M.H. Thiemens, Geoph. Res. Lett. **15**, No. 1, 9 (1988).
92. K. Mauersberger, J. Morton, B. Schuler, et al., in: *Abstracts of Reports at Quadr. Ozone Symposium* Charlottesville, Virginia (1992).
93. D.R. Bates, J. Chem. Phys. **93**, No. 3, 2158; No. 12, 8739 (1990).
94. S.M. Anderson, J. Morton, and K. Mauersberger, Chem. Phys. Lett. **156**, No. 2/3, 175 (1989).
95. D.R. Bates, Geoph. Res. Lett. **15**, No. 1, 13 (1988).
96. S.M. Anderson, J. Morton, K. Mauersberger, et al., Chem. Phys. Lett. **189**, No. 6, 581 (1992).
97. W.B. DeMore, M.J. Molina, S.P. Sander, et al.: in: NASA Panel for Data Evaluation, Chemical Kinetics and Photochemical DATA for Use on Stratospheric Modeling, Evaluation Number 8, JPL Publ., 87–41 (1987).